https://doi.org/10.5194/egusphere-2026-4623
Preprint. Discussion started: 10 August 2026

Quantifying the Southern Ocean pCO_2 sampling error with synthetic observations from an ocean model

Cara Nissen[1,2], Alison R. Gray[3], Nicole S. Lovenduski[2], Mathew Maltrud[4], and LeAnn Conlon[4]

[1]Department of Freshwater and Marine Ecology, Institute for Biodiversity and Ecosystem Dynamics, University of Amsterdam, Amsterdam, the Netherlands
[2]Department of Atmospheric and Oceanic Sciences and Institute of Arctic and Alpine Research, University of Colorado, Boulder, Boulder, CO, USA
[3]School of Oceanography, University of Washington, Seattle, WA, USA
[4]Fluid Dynamics and Solid Mechanics (T-3), Los Alamos National Laboratory, Los Alamos, NM, USA

Correspondence: Cara Nissen (c.nissen@uva.nl)

Abstract. Constraining the Southern Ocean carbon sink is vital for understanding global carbon cycling and climate. Monthly 1°x1° gridded products of surface seawater partial pressure of carbon dioxide (pCO_2) are routinely used to detect change in Southern Ocean carbon cycling. Despite Southern Ocean sampling being sparse and skewed to summer months, the uncertainty arising from incomplete sampling at the monthly 1°x1° scale is unquantified to date, and it remains unclear how this pCO_2 sampling error affects estimates of monthly gridded pCO_2 products and derived air-sea CO_2 fluxes. Here, we quantify the Southern Ocean pCO_2 sampling error using synthetic observations from an eddy-permitting ocean-sea ice-biogeochemistry configuration of the Energy Exascale Earth System Model. Using instantaneous snapshots of the model state at the times and locations of real-world ship and float observations, we reconstruct gridded monthly 1°x1° pCO_2 datasets over 2014-2023 and compare them with the simulated model pCO_2 output, isolating the error due to incomplete observational coverage at the monthly 1°x1° scale. We find that, on average, pCO_2 derived from synthetic observations is 13-14 μatm lower than the modeled monthly mean, with individual grid cells exhibiting uncertainties up to an order of magnitude larger, primarily caused by undersampling during high-wind events in the Southern Ocean. Our results imply that the rate of oceanic CO_2 uptake derived from available pCO_2 observations is biased high. Since the pCO_2 uncertainty due to incomplete observational coverage exceeds other sources of uncertainty in gridded pCO_2 data products, e.g., measurement error, it represents a substantial, previously overlooked contribution that should be propagated through gap-filled pCO_2 data products and estimates of the Southern Ocean and global ocean carbon sink.

1 Introduction

The Southern Ocean south of 40°S contributes disproportionately to global carbon cycling (DeVries et al., 2023; Hauck et al., 2023a; Friedlingstein et al., 2026), making it crucial to improve our ability to robustly quantify Southern Ocean carbon distributions for the detection of climate-relevant trends. Recurring efforts to establish regional Southern Ocean (Hauck et al., 2023a) and global carbon budgets (DeVries et al., 2023; Friedlingstein et al., 2026) use a combination of process-based ocean

https://doi.org/10.5194/egusphere-2026-4623
Preprint. Discussion started: 10 August 2026

models and gap-filled observation-based data products of the surface seawater partial pressure of carbon dioxide (pCO$_2$) to quantify the Southern Ocean carbon sink. While the large spread across ocean models remains a concern (Friedlingstein et al., 2026), pCO$_2$ data products based on surface seawater observations of the fugacity of CO$_2$ (fCO$_2$) are sensitive to measurement accuracy, sampling distributions, and methods used to fill gaps in coverage (e.g., Bakker et al., 2016; Bushinsky et al., 2019; Hauck et al., 2023b; Dong et al., 2024; Fay et al., 2025). Surface seawater fCO$_2$ observations, mainly collected from ships, are regularly aggregated into a gridded fCO$_2$ data product, i.e., observations are bin-averaged in 1°x1° grid boxes for each month, in the Surface Ocean CO$_2$ ATlas (SOCAT; Bakker et al., 2016). Gridded SOCAT products then form the basis for machine learning methods that extrapolate available Southern Ocean fCO$_2$ observations to basin-wide pCO$_2$ data products for use in carbon budgets (e.g., Landschützer et al., 2013).

This approach assumes current observational coverage to be sufficient to capture all spatial and temporal scales relevant for basin-scale surface pCO$_2$ variability. While gridded SOCAT and gap-filled pCO$_2$ data products focus on the seasonal time scale and the 1°x1° spatial scale (Bakker et al., 2016; Friedlingstein et al., 2026), Southern Ocean surface pCO$_2$ is highly variable on shorter time scales (Monteiro et al., 2015; Djeutchouang et al., 2022; Nicholson et al., 2022; Shadwick et al., 2023; Gregor et al., 2024; Robache and Schmitt, 2026) and smaller spatial scales (Nicholson et al., 2022; Gregor et al., 2024; Patara et al., 2026). Even at monthly 1°x1° resolution, large parts of the open Southern Ocean south of 40°S remain unobserved by ships between 2014 and 2023 (Fig. 1a), and ship-based data are biased towards summer months (Fig. 2b) and non-stormy conditions (Bakker et al., 2016). While autonomously profiling biogeochemical (BGC) Argo floats have added substantial spatial coverage since 2014 (Sarmiento et al., 2023) (Fig. 1b & Fig. 2a,b), these data are not currently included in SOCAT due to uncertainties associated with the conversion of float-based pH measurements to seawater fCO$_2$ or pCO$_2$ (Williams et al., 2017; Gray et al., 2018; Zhang et al., 2026). Importantly, for the majority of monthly 1°x1° grid cells with at least one observation in the SOCAT or BGC Argo-pH database, less than half of the days in each month and hours in each day are sampled (Fig. 2c,d), highlighting the incomplete sampling coverage across the Southern Ocean.

Due to this incomplete sampling coverage, we do not know the true monthly mean pCO$_2$ in any 1°x1° grid cell for the real ocean. In contrast, pCO$_2$ is predicted everywhere and at all time steps in ocean models, and synthetic observations from ocean models are thus a viable alternative to assess the impact of incomplete sampling coverage on basin-scale estimates of pCO$_2$. Using ocean models as a testbed, many studies have demonstrated how additional Southern Ocean sampling coverage can reduce uncertainties in basin-scale estimates of air-sea CO$_2$ fluxes derived from pCO$_2$ (e.g., Bushinsky et al., 2019; Hauck et al., 2023b; Heimdal et al., 2024; Heimdal and McKinley, 2024; Behncke et al., 2024, 2026). In such model subsampling exercises, synthetic pCO$_2$ observations are extracted from time-averaged model output, most often at monthly 1°x1° resolution, in line with the resolution of gridded SOCAT products (Bakker et al., 2016, 2024). This approach allows for easy comparison across models, mapping methods, and different scenarios of sampling coverage (Hauck et al., 2023b; Roobaert et al., 2026), while acknowledging the remaining uncertainty when translating findings from model subsampling exercises to the real ocean due to model biases or incomplete representation of key processes (e.g., Bellenger et al., 2023; Hauck et al., 2023a; Roobaert et al., 2026). However, this approach assumes sampling coverage within each monthly 1°x1° grid cell to be perfect, and thus cannot quantify how incomplete sampling coverage at the monthly 1°x1° scale affects basin-scale pCO$_2$ reconstructions.

https://doi.org/10.5194/egusphere-2026-4623
Preprint. Discussion started: 10 August 2026

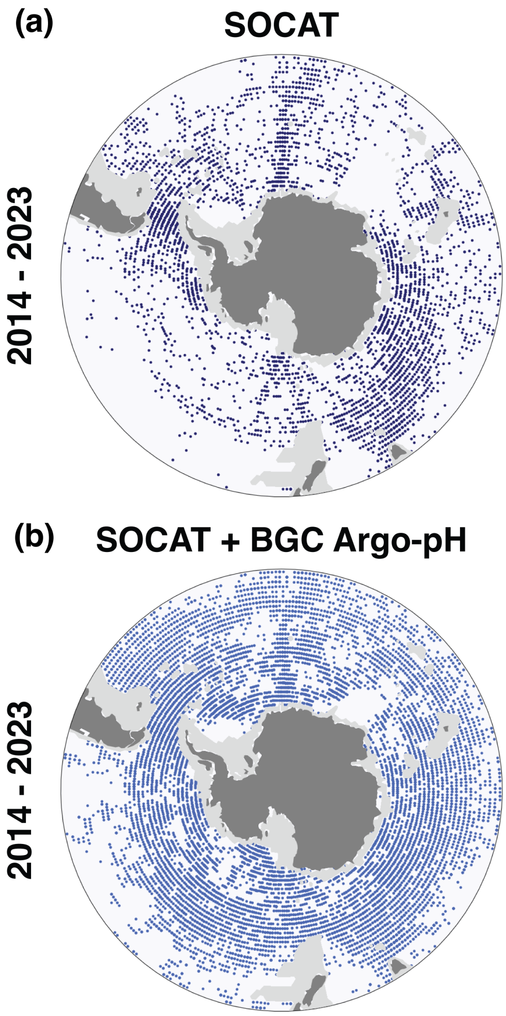

Figure 1. Spatial data availability in SOCAT and BGC Argo-pH in the open Southern Ocean south of 40°S used here for the quantification of $p\mathrm{CO_2}$ sampling error. Maps show monthly 1°x1° grid cells in waters deeper than 2000 m between 2014 and 2023 that contain at least one observation from (a) the SOCAT database and (b) the combined SOCAT and BGC Argo-pH dataset. Regions shallower than 2000 m are shown in light grey. See also section 2.2.

https://doi.org/10.5194/egusphere-2026-4623
Preprint. Discussion started: 10 August 2026

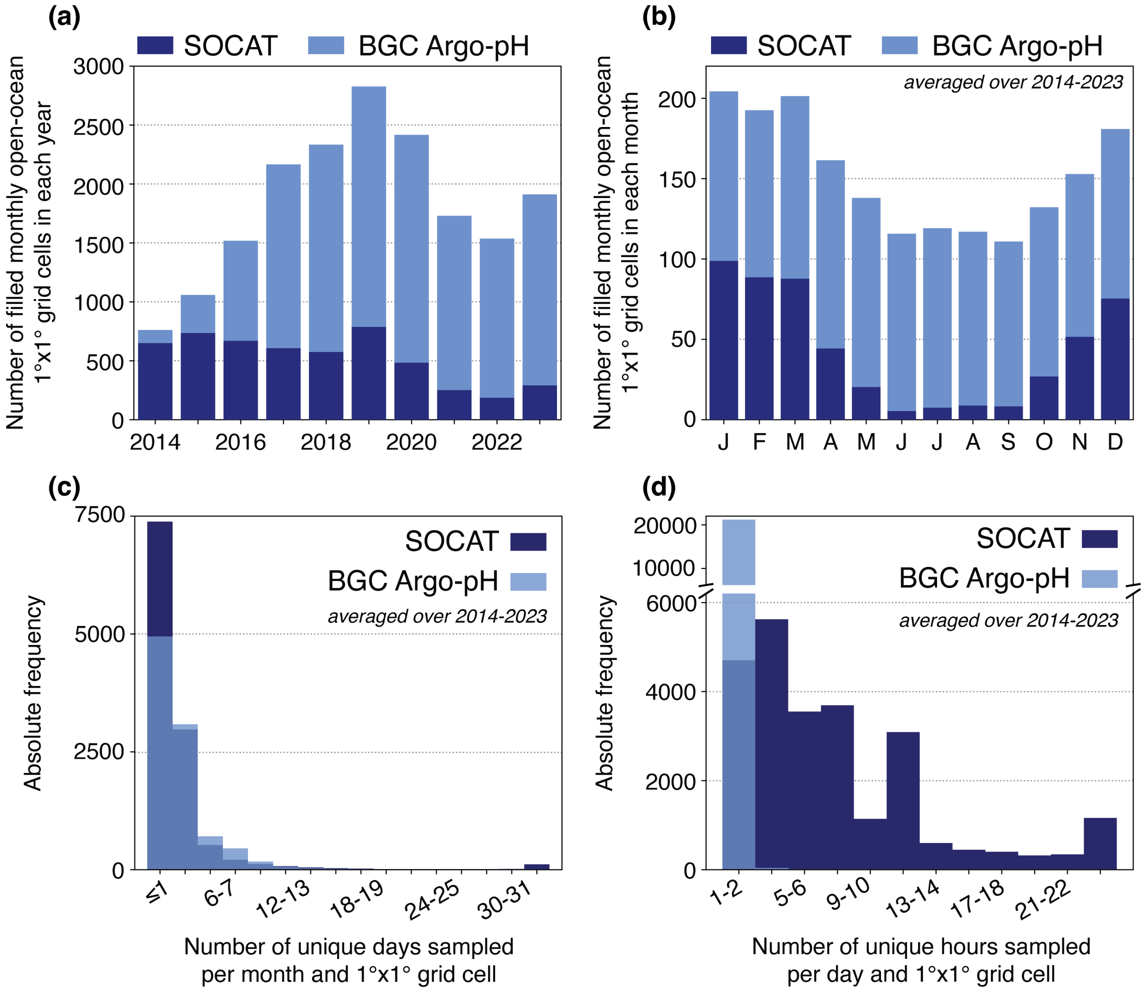

Figure 2. Temporal data availability in SOCAT and BGC Argo-pH in the Southern Ocean south of 40°S. Number of monthly 1°x1° grid cells that contain at least one observation (a) for each year between 2014 and 2023 and (b) for each month (averaged over 2014-2023). SOCAT and BGC Argo-pH are shown in dark blue and light blue, respectively. Panels (c) and (d) show the absolute frequency distribution of how many (c) unique days per month and (d) unique hours per day are sampled in the two databases for any given monthly 1°x1° grid cell averaged over 2014-2023. Only grid cells in waters deeper than 2000 m are included.

https://doi.org/10.5194/egusphere-2026-4623
Preprint. Discussion started: 10 August 2026

Given the historically incomplete sampling coverage in the Southern Ocean (Figs. 1 & 2) and the known high spatio-temporal variability of surface $p\mathrm{CO_2}$ (e.g., Eveleth et al., 2017; Nicholson et al., 2022; Gregor et al., 2024), it is critical to quantify this $p\mathrm{CO_2}$ sampling error.

Here, we quantify the Southern Ocean $p\mathrm{CO_2}$ sampling error using synthetic observations from the Energy Exascale Earth System Model version 2 (E3SMv2; Nissen et al., 2024; Christensen et al., 2026). The synthetic observations are generated during model integration on an eddy-permitting grid with 10-15 km horizontal resolution in the Southern Ocean, providing 4-hourly snapshots of the simulated surface ocean $p\mathrm{CO_2}$. We define the $p\mathrm{CO_2}$ sampling error as the discrepancy between the surface $p\mathrm{CO_2}$ obtained from synthetic observations at historical sampling sites and the true modeled $p\mathrm{CO_2}$ value in each monthly 1°x1° grid cell. We quantify the benefit of incorporating BGC Argo-pH observations into gridded monthly $p\mathrm{CO_2}$ products by comparing a synthetic SOCAT-only dataset with one that merges SOCAT with available BGC Argo-pH observations.

2 Methods

2.1 E3SM with Lagrangian floats

To recreate gridded surface seawater $p\mathrm{CO_2}$ datasets, we use the synthetic biogeochemical float capabilities, LIGHT-bgcArgo-1.0, in the ocean component of the E3SMv2 (Nissen et al., 2024). The Model for Prediction Across Scales – Ocean (MPAS-O), and the Model for Prediction Across Scales – Sea Ice (MPAS-Seaice) make up the physical ocean and sea-ice model components of E3SMv2 (Petersen et al., 2019; Golaz et al., 2022; Turner et al., 2022). Both components are run on unstructured multi-resolution model grids with hexagonal grid cells (Ringler et al., 2013). Ocean biogeochemistry, including carbon cycling, is simulated with the Marine Biogeochemistry Library (MARBL; Long et al., 2021). LIGHT-bgcArgo-1.0 builds on the online Lagrangian, In situ, Global, High-performance particle Tracking (LIGHT) module developed by Wolfram et al. (2015) and is described in more detail in Nissen et al. (2024). In short, synthetic biogeochemical floats are advected with the simulated ocean circulation at 1000 m and sample the whole water column online, i.e. during model integration, at a user-defined frequency. These synthetic floats thus provide the same snapshot view of simulated physical, chemical, and biological ocean properties as real-world observations do of the real ocean.

For this study, we use the same forced ocean-sea ice simulation as Christensen et al. (2026). The grid for MPAS-O and MPAS-Seaice in this simulation has eddy-permitting resolution within and south of the Antarctic Circumpolar Current (10-15 km) and coarser resolution north of 40°S (>50 km; Fig. 3a). At the ocean surface, the simulation is forced with three-hourly atmospheric fields at ∼0.56° horizontal resolution from the Japanese atmospheric reanalysis (1958-2023; Tsujino et al., 2018). After 122 years of spinup, more than 1800 synthetic biogeochemical floats are deployed in the modeled Southern Ocean south of 40°S on January 1, 1980 (Fig. 3a). These floats instantaneously sample the whole water column every four hours through the end of 2023, recording a range of model prognostic and diagnostic variables. Here, we use model-derived synthetic observations of surface seawater $p\mathrm{CO_2}$ to assess the $p\mathrm{CO_2}$ sampling error by comparing the synthetic observations to the Eulerian $p\mathrm{CO_2}$ fields in a given grid cell (see section 2.2). To that aim, the simulated monthly Eulerian fields of surface seawater $p\mathrm{CO_2}$ are interpolated to a regular 1°x1° grid using bilinear interpolation. Since the synthetic float network is both dense and samples

https://doi.org/10.5194/egusphere-2026-4623
Preprint. Discussion started: 10 August 2026

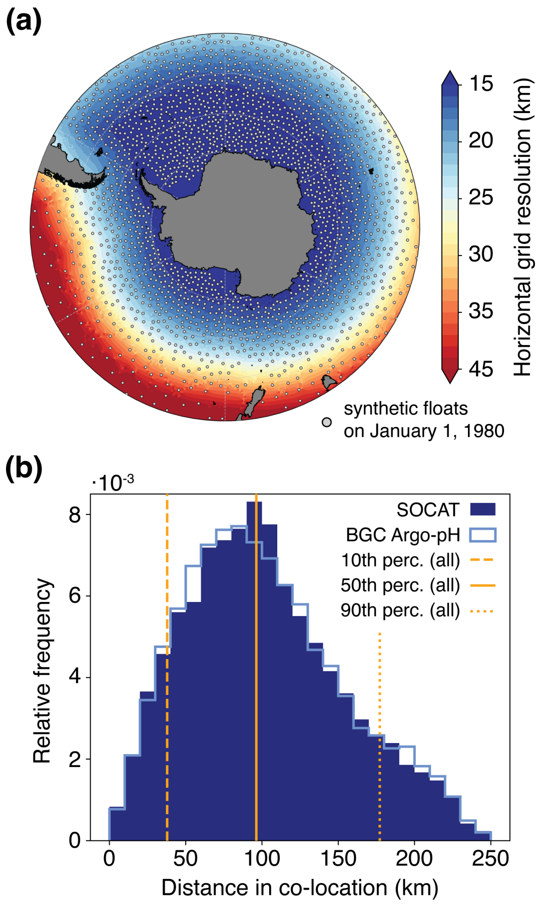

Figure 3. (a) Spatial distribution of synthetic floats in E3SM in the Southern Ocean south of 40°S on January 1, 1980 (initialization). Background colors indicate the native horizontal grid resolution (km) of the underlying ocean model. (b) Relative frequency distribution of co-location distances (km) between each SOCAT (dark blue) and BGC Argo-pH (light blue) observation and its nearest synthetic E3SM float between 2014 and 2023. Only observations in waters deeper than 2000 m are included. Vertical orange lines indicate the 10^{th} (dashed), 50^{th} (solid), and 90^{th} (dotted) percentile of the combined SOCAT and BGC Argo-pH dataset.

https://doi.org/10.5194/egusphere-2026-4623
Preprint. Discussion started: 10 August 2026

at high temporal frequency, we exploit these characteristics to treat it as a multi-platform observing system. This allows us to reconstruct not only float-based but also ship-based carbon observational datasets to quantify the Southern Ocean $p\mathrm{CO_2}$ sampling error.

2.2 Recreating gridded $p\mathrm{CO_2}$ datasets with synthetic observations

For this study, we define the $p\mathrm{CO_2}$ sampling error as the difference between the surface seawater $p\mathrm{CO_2}$ obtained from averaging all available synthetic $p\mathrm{CO_2}$ observations for a given monthly 1°x1° grid cell and the modeled $p\mathrm{CO_2}$ value of that grid cell. A negative $p\mathrm{CO_2}$ sampling error thus means that incomplete spatial or temporal sampling coverage in a grid cell results in estimates of $p\mathrm{CO_2}$ that are too low, implying that oceanic $\mathrm{CO_2}$ uptake derived from these values is too large. To recreate gridded surface seawater $p\mathrm{CO_2}$ datasets, we use historical sampling distributions in the Southern Ocean south of 40°S from i) ship-based observations in SOCAT v2024 (Sabine et al., 2013; Bakker et al., 2016, 2024) and ii) SOCAT merged with available BGC Argo-pH observations (Argo, 2024). To quantify the effect of sampling distributions on the simulated $p\mathrm{CO_2}$ sampling error, we restrict the analysis to available model years after the first Southern Ocean biogeochemical float deployment, i.e., 2014-2023. In this study, we assume that both ship-based and float-based observations yield perfect estimates of seawater $p\mathrm{CO_2}$. Thus, our analysis only focuses on the uncertainty due to incomplete sampling coverage. We acknowledge that, in the real ocean, merging SOCAT and BGC-Argo observations introduces uncertainties arising from sensor inaccuracies and from the derivation of $p\mathrm{CO_2}$ based on float-measured pH and estimated alkalinity determined empirically from temperature, salinity, and oxygen (Bakker et al., 2016; Williams et al., 2017; Gray et al., 2018; Zhang et al., 2026).

The recreation of the gridded $p\mathrm{CO_2}$ datasets with synthetic observations from E3SM proceeds in three steps. First, since E3SM only simulates profiling floats in the open ocean (Fig. 3a), $p\mathrm{CO_2}$ sampling locations in waters shallower than 2000 m are excluded from the SOCAT dataset. While all available BGC Argo-pH observations are retained in this step (22,233 for 2014-2023), only 1,784,523 (53.2%) of the originally 3,355,331 $p\mathrm{CO_2}$ observations in the SOCAT dataset are located in open-ocean waters. Next, each historical SOCAT and BGC Argo-pH observation is co-located with a synthetic E3SM observation by minimizing the spatial (latitude, longitude) and temporal (year, month, day, hour) separation between the real and synthetic measurements. Given the 4-hour sampling frequency of the synthetic E3SM observations in the simulation used here (see section 2.1), the real and synthetic measurements differ by at most two hours in time, which ensures that diurnal coverage is preserved. In space, the distance between the real and synthetic measurements differs more widely (up to 250 km; Fig. 3b). To preserve the spatial coverage of SOCAT and BGC Argo-pH as much as possible, we require the co-located synthetic observation to be within a 2° radius of any real observation, and we exclude any observation that cannot be matched under this condition. This step reduces the input data points to 45.8% (1,536,086) and 86.7% (19,278) of all available Southern Ocean observations for SOCAT and BGC Argo-pH, respectively. The merged dataset thus includes 1,555,364 $p\mathrm{CO_2}$ synthetic observations. We note that while the quantitative results in this study are sensitive to the data reduction in this second step, the qualitative results are insensitive to this choice. In the last step, the synthetic E3SM observations are aggregated into monthly 1°x1° grid cells by averaging all co-located synthetic observations that were assigned the same monthly 1°x1° grid cell. Importantly, when multiple historical sampling locations were assigned the same synthetic observation in the second step

https://doi.org/10.5194/egusphere-2026-4623
Preprint. Discussion started: 10 August 2026

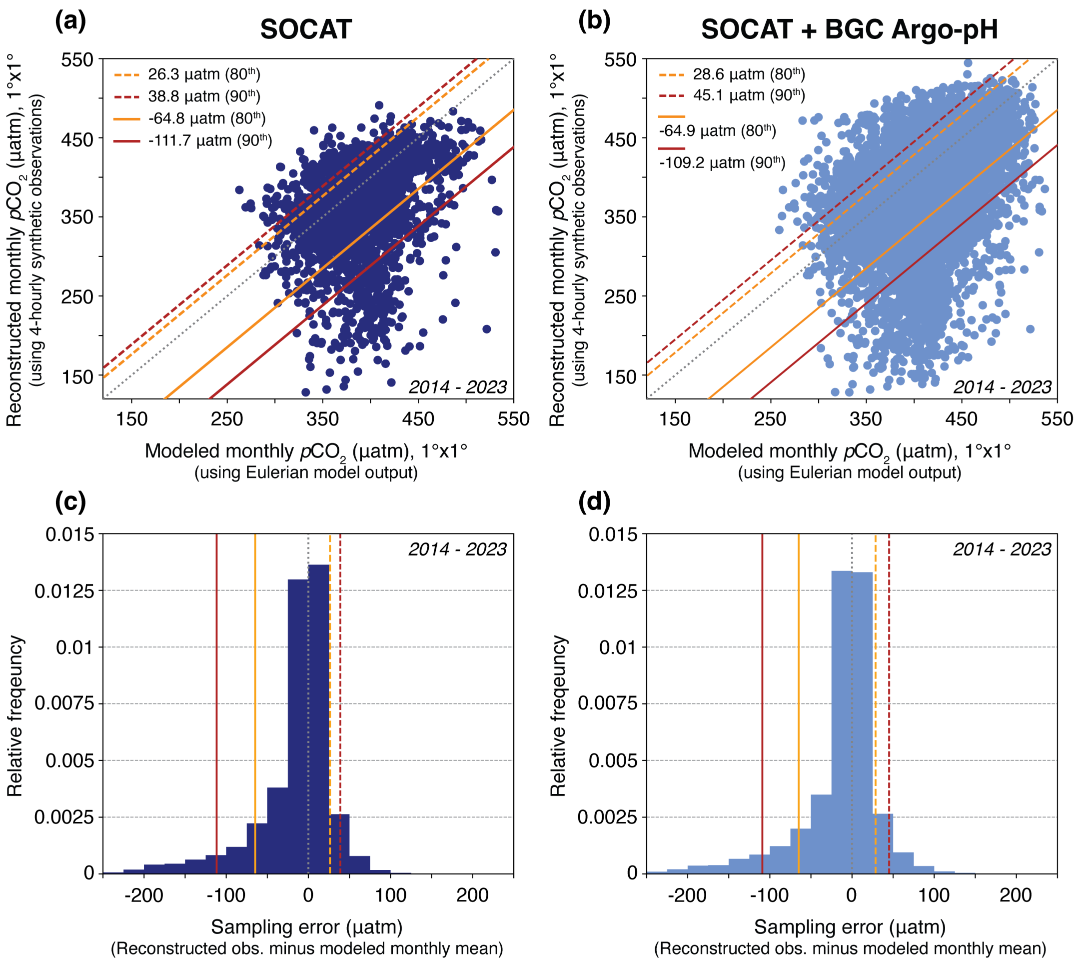

Figure 4. Surface seawater pCO_2 sampling error in the Southern Ocean south of 40°S. Comparison of surface seawater pCO_2 (μatm) in all monthly 1°x1° grid cells 2014-2023 that contain at least one observation between the true time-averaged E3SM model output ("modeled pCO_2") and the reconstructed synthetic observations that account for historical coverage and sub-monthly as well as sub–grid cell variability ("reconstructed pCO_2") in (a, c) SOCAT and (b, d) the merged SOCAT and BGC Argo-pH dataset. In each panel, the difference between the reconstructed observations and modeled monthly mean pCO_2 estimates defines the pCO_2 sampling error. The dotted grey line indicates zero sampling error, while colored lines highlight grid cells with sampling error exceeding the 80^{th} (orange) and 90^{th} (red) percentile shown separately for positive (dashed) and negative (solid) sampling errors.

https://doi.org/10.5194/egusphere-2026-4623
Preprint. Discussion started: 10 August 2026

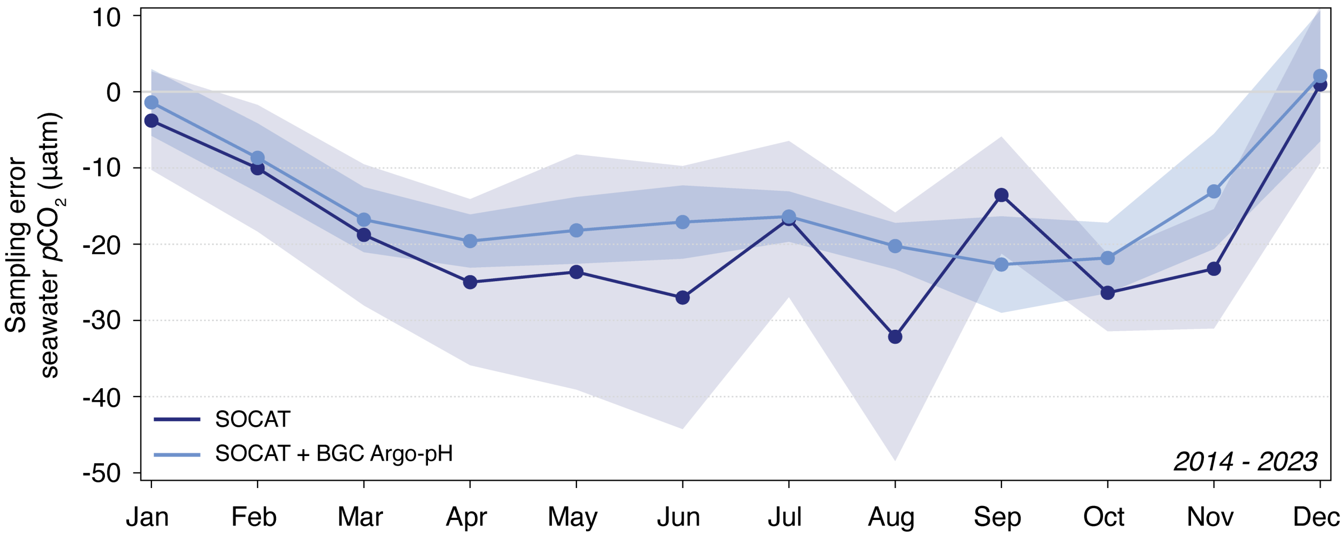

Figure 5. Seasonal evolution of the surface seawater pCO_2 sampling error in the Southern Ocean south of 40°S. The sampling error (μatm) is defined as the difference in surface seawater pCO_2 between the modeled monthly mean E3SM model output (x axis in Fig. 4a, b) and the reconstructed synthetic observations based on historical coverage (y axis in Fig. 4a, b). After calculating the sampling error for each monthly 1°x1° grid cell (Fig. 4), the errors are here averaged for each month and year, accounting for differences in area coverage. Solid lines show the monthly mean for SOCAT (dark blue) and the merged SOCAT and BGC Argo-pH dataset (light blue) averaged over all years (2014-2023), and shading indicates interannual variability, expressed as one standard deviation around the mean of all years.

(identical latitude, longitude, year, month, day, and hour), that synthetic data point was included only once in the averaging. This avoids overweighting frequent, potentially correlated pCO_2 measurements from ship-based underway observations, following a procedure analogous to that used for SOCAT (Bakker et al., 2016). Following these steps, 5,171 and 18,076 monthly 1°x1° grid cells contain a pCO_2 estimate for SOCAT and the merged SOCAT and BGC Argo-pH dataset, respectively, in the gridded pCO_2 datasets recreated with synthetic E3SM observations (Fig. 1). For the years 2014-2023, this corresponds to a coverage of 0.44% (SOCAT only) and 1.54% (merged dataset) of all open-ocean monthly 1°x1° grid cells.

3 Results

3.1 Simulated pCO_2 sampling error in E3SM

The simulated pCO_2 sampling error varies greatly across monthly 1°x1° grid cells that contain at least one observation. For SOCAT, the pCO_2 estimated from the synthetic observations ("reconstructed pCO_2") is between 244 μatm lower and 70 μatm higher than the monthly mean model truth ("modeled pCO_2"; Fig. 4a, c). For the merged SOCAT and BGC Argo-pH dataset, this range increases to 418 μatm lower and 70 μatm higher (Fig. 4b, d). Overall, the statistics for the grid cells with the largest sampling error are similar for both datasets. For SOCAT, 20% of all grid cells exhibit sampling errors smaller than -65 μatm

https://doi.org/10.5194/egusphere-2026-4623
Preprint. Discussion started: 10 August 2026

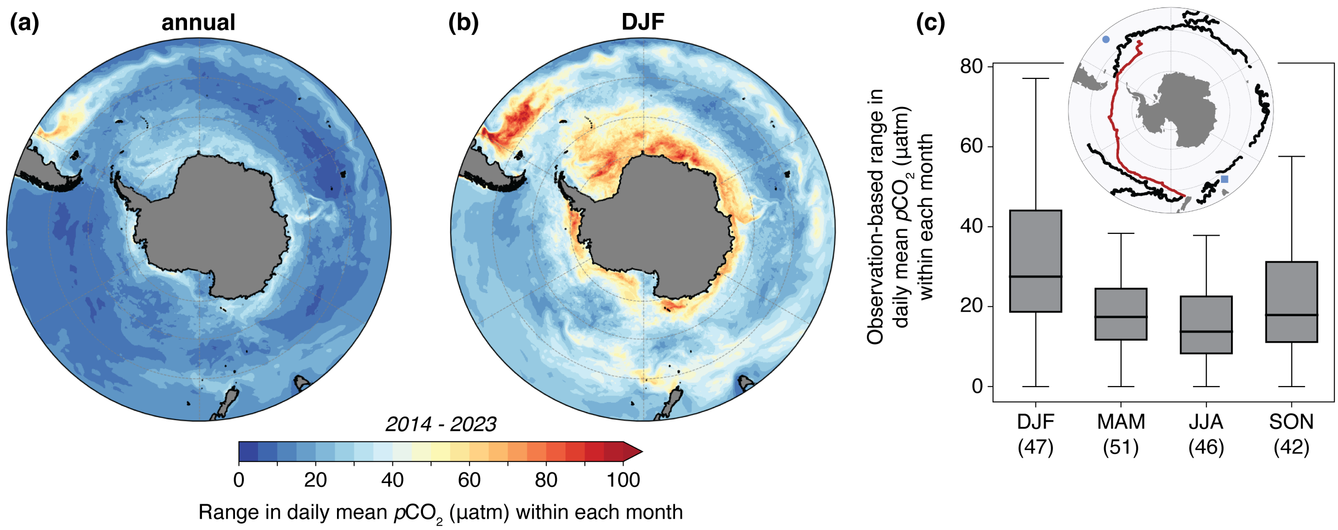

Figure 6. Sub-monthly variability. Maps of the range in simulated daily average surface seawater pCO_2 (μatm) in E3SM within each month for 2014-2023, averaged (a) over all months and (b) over summer months only (December-February, DJF). Panel (c) shows box plots of observation-based ranges in the Southern Ocean south of 40°S for summer (DJF), fall (MAM), winter (JJA), and spring (SON). Inlet shows the buoy trajectories (lines) and the location of buoys (symbols). Data are from Sutton et al. (2021, red line), Robache and Schmitt (2026, black lines), Sutton et al. (2014, blue square) and OOI (2015, blue circle).

and larger than 26 μatm, respectively (Fig. 4a, c), and these thresholds change only slightly with the addition of BGC Argo-pH (-65 μatm and 29 μatm; Fig. 4b, d). Averaged over all monthly 1°x1° grid cells with at least one observation, the pCO_2 sampling error amounts to -14.1 μatm for SOCAT and to -13.5 μatm for the merged dataset. This indicates that between 2014 and 2023, the inclusion of BGC Argo-pH did not provide sufficient additional spatio-temporal coverage to substantially reduce the sampling error in the simulated monthly, 1°x1° gridded pCO_2 dataset in E3SM.

The benefit of including BGC Argo-pH data becomes evident when examining the pCO_2 sampling error across seasons and years. During summer (December-February), the average pCO_2 sampling error is fairly close to zero for both datasets (-4.3 μatm for SOCAT and -2.7 μatm for the merged SOCAT and BGC Argo-pH dataset); it can even be positive in some years (see shading in Fig. 5). However, for all non-summer months, the mean pCO_2 sampling error is negative and has a magnitude larger than 10 μatm in most years (Fig. 5). Overall, the addition of BGC Argo-pH observations leads to two major improvements: i) a 29% improvement in the pCO_2 sampling error in winter months (June-August; -25.3 μatm as compared to -17.9 μatm) and ii) a reduction in the simulated spread in the pCO_2 sampling error across years (compare dark blue and light blue shading in Fig. 5). The latter results from enhanced coverage with BGC Argo-pH, especially in winter; for June-August between 2014 and 2023, 94% of all grid cells with at least one observation can be attributed to the addition of BGC Argo-pH (light blue in Fig. 2b).

https://doi.org/10.5194/egusphere-2026-4623
Preprint. Discussion started: 10 August 2026

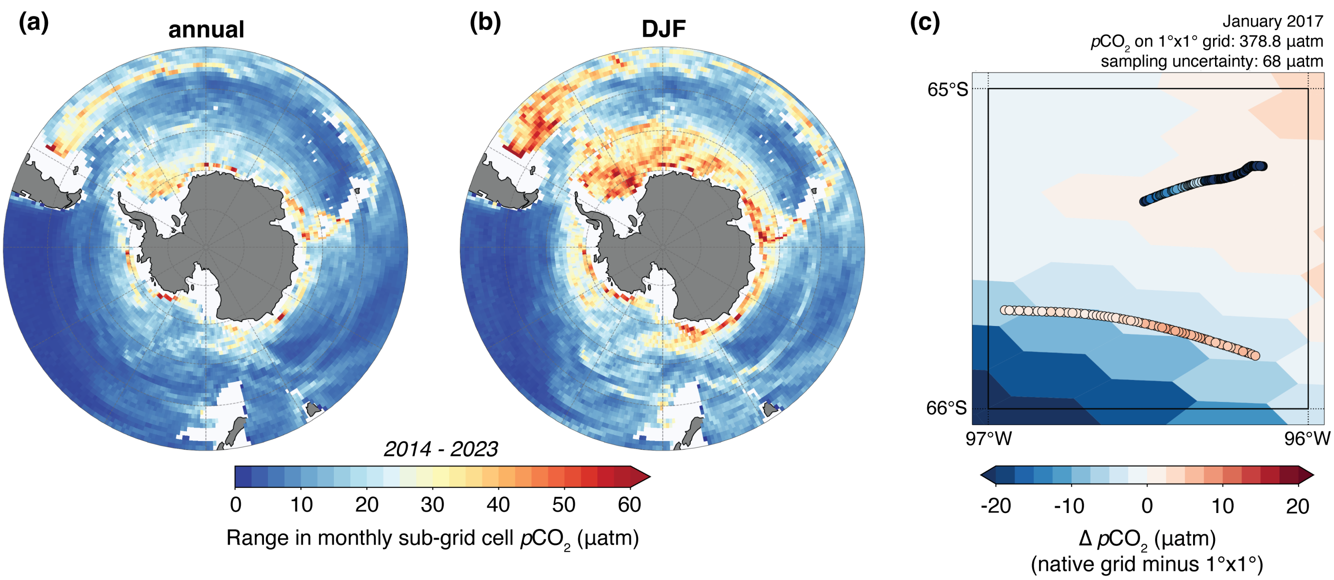

Figure 7. Sub-grid cell variability. Maps of E3SM surface seawater pCO$_2$ variability (μatm) within each 1°x1° grid cell for 2014-2023, averaged (a) over all months and (b) over summer months only (December-February, DJF). Sub-grid cell variability is here defined as the range in monthly pCO$_2$ across all native model grid cells contained within each 1°x1° grid cell. Panel (c) illustrates a single 1°x1° grid cell in January 2017, with background colors showing the difference between the monthly mean pCO$_2$ on the regular grid (378.8 μatm) and pCO$_2$ in each native model grid cell. All available synthetic float observations within this monthly grid cell are also shown, with colors denoting the difference to the monthly mean pCO$_2$ on the regular grid.

3.2 Simulated spatio-temporal pCO$_2$ variability in E3SM

The spatio-temporal pCO$_2$ variability within a 1°x1° grid cell dictates how many observations are required to adequately capture the true monthly pCO$_2$ at that location. In E3SM, simulated seawater pCO$_2$ displays large variability within any 1°x1° grid cell and month (Figs. 6 & 7). Expressing sub-monthly variability as the range in daily mean pCO$_2$ for a given month, the temporal pCO$_2$ variability in E3SM locally exceeds 50 μatm for the annual mean and 100 μatm for the summer mean (December-February; Fig. 6a, b). While large parts of the open ocean show values below 20 μatm and 40 μatm, respectively, areas of highest variability are found off the Patagonian shelf and at latitudes >60°S. These regions broadly coincide with areas of high variability in biological productivity and sea-ice cover (not shown), possibly explaining the large sub-monthly pCO$_2$ variability especially during summer. Recognizing the scarcity of observational data at high-enough temporal frequency across the Southern Ocean to evaluate the simulated sub-monthly pCO$_2$ variability, the simulated range in daily mean pCO$_2$ compares reasonably well to that derived from available open-ocean measurements from moorings, drifting buoys, and an uncrewed surface vehicle (Fig. 6c; OOI, 2015; Sutton et al., 2014, 2021; Robache and Schmitt, 2026). While we cannot quantify diurnal pCO$_2$ variability in the Eulerian model output because sub-daily output was not stored, the median diurnal pCO$_2$ cycle in E3SM based on all available synthetic observations at 4-hourly frequency ranges from 0.5 to 2.4 μatm across seasons (with a

https://doi.org/10.5194/egusphere-2026-4623
Preprint. Discussion started: 10 August 2026

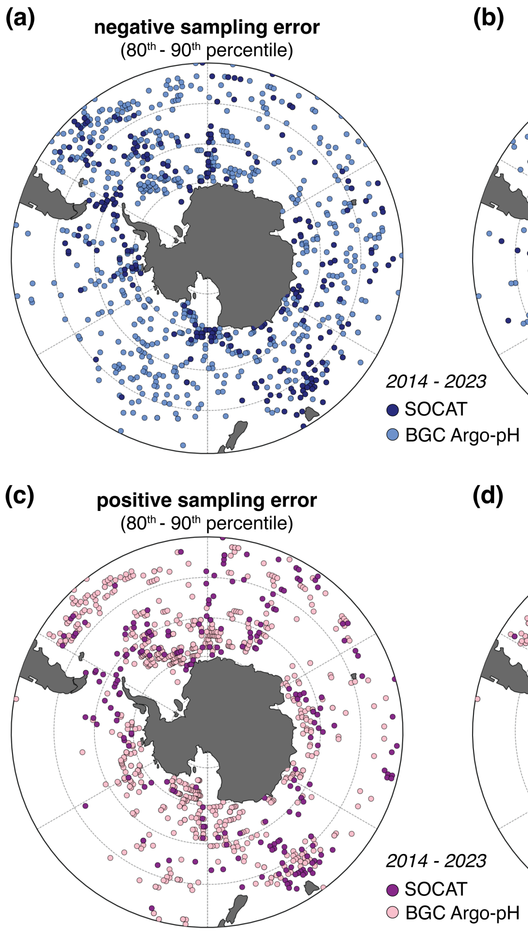

Figure 8. Spatial distribution of large surface seawater $p\mathrm{CO_2}$ sampling errors in the Southern Ocean south of 40°S. Maps indicate locations of sampling errors (a, c) within the 80-90$^{\mathrm{th}}$ percentile range and (b, d) exceeding the 90$^{\mathrm{th}}$ percentile. Results are shown separately for (a,b) negative and (c,d) positive sampling error. Darker and lighter colors denote SOCAT and the merged SOCAT and BGC Argo-pH dataset, respectively. For thresholds of $p\mathrm{CO_2}$ sampling errors used here, see Fig. 4b.

https://doi.org/10.5194/egusphere-2026-4623
Preprint. Discussion started: 10 August 2026

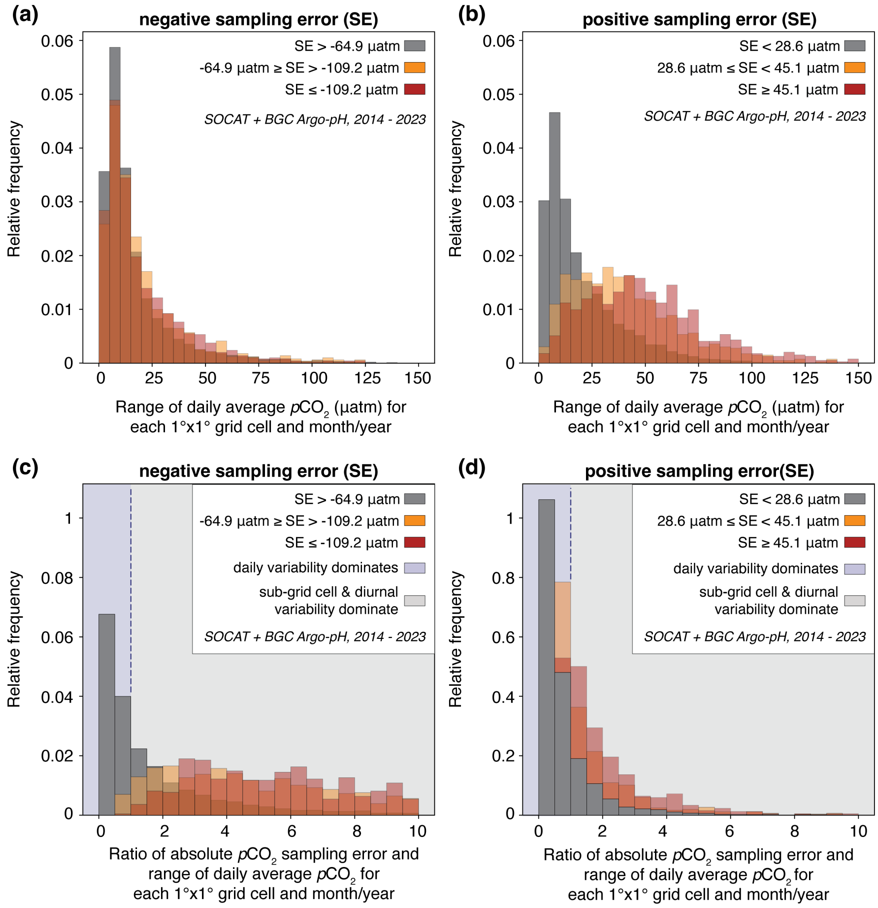

Figure 9. Relating surface seawater pCO_2 sampling error (SE) to simulated pCO_2 variability. Relative frequency distribution for the merged SOCAT and BGC Argo-pH synthetic dataset for 2014-2023 of (a, c) negative and (b, d) positive pCO_2 sampling errors. Sampling errors are related to (a, b) the range in daily mean pCO_2 (μatm) for each location and time (see also Fig. 6) and (c, d) the ratio of the absolute sampling error to the range in daily mean pCO_2. For panels (c, d), a ratio <1 indicates that daily pCO_2 variability exceeds the sampling error (blue area), whereas a ratio >1 highlights cases where sub-grid cell or diurnal variability dominate (grey area). In all panels, colors distinguish small ($<80^{th}$ percentile) from large ($\geq 80^{th}$ percentile) pCO_2 sampling error; thresholds are the same as in Fig. 4.

https://doi.org/10.5194/egusphere-2026-4623
Preprint. Discussion started: 10 August 2026

maximum of 148.4 μatm), which adds to the sub-monthly variability shown in Fig. 6. Acknowledging that large parts of the Southern Ocean remain unobserved at this temporal frequency, the simulated diurnal cycles are in line with observation-based estimates (median range 4.6-7.1 μatm, maximum 101.2 μatm; Sutton et al., 2014; Robache and Schmitt, 2026).

Simulated $p\mathrm{CO_2}$ variability at spatial scales smaller than 1°x1° exhibits similar patterns as sub-monthly temporal variability but is smaller in magnitude compared to the simulated sub-monthly variability. Expressing the sub-grid cell $p\mathrm{CO_2}$ variability as the range in monthly mean $p\mathrm{CO_2}$ across all native grid cells within each 1°x1° grid cell, the spatial $p\mathrm{CO_2}$ variability in E3SM exceeds 30 μatm for the annual mean and 60 μatm for the summer mean (December-February; Fig. 7a, b). In large parts of the open ocean, the spatial $p\mathrm{CO_2}$ variability is below 10 μatm and 20 μatm, respectively, while the regions downstream of the Patagonian shelf and at high latitudes exhibit the highest values. Altogether, the magnitude of the simulated $p\mathrm{CO_2}$ sampling error is in line with the simulated spatio-temporal $p\mathrm{CO_2}$ variability, suggesting that inadequate observational coverage in a monthly 1°x1° grid cell can lead to large sampling errors. This is further illustrated by the example 1°x1° grid cell from the high-latitude South Pacific in Fig. 7c, which highlights the mismatch between the simulated monthly mean $p\mathrm{CO_2}$ for all native grid cells (background), available synthetic float observations (dots), and the true monthly mean $p\mathrm{CO_2}$.

3.3 Relating spatio-temporal $p\mathrm{CO_2}$ variability to the $p\mathrm{CO_2}$ sampling error

Relating spatio-temporal $p\mathrm{CO_2}$ variability to the $p\mathrm{CO_2}$ sampling error gives insights into the adequacy of current sampling efforts in regions of high or low $p\mathrm{CO_2}$ variability. In E3SM, the spatial distribution of the monthly 1°x1° grid cells with the largest 20% $p\mathrm{CO_2}$ sampling error differs between locations with negative and positive sampling error, i.e., where the gridded value is lower (negative) or higher (positive) than the modeled monthly mean (compare top row to bottom row in Fig. 8). Irrespective of whether considering only SOCAT or the merged dataset, locations with a large negative sampling error are generally more widespread than those with a large positive sampling error (Fig. 8). For the latter, most locations are clustered at high latitudes, off the Patagonian Shelf and south of Tasmania (Fig. 8c, d). Interestingly, these clusters broadly align with elevated spatio-temporal $p\mathrm{CO_2}$ variability (Figs. 6 & 7). For all grid cells with a positive $p\mathrm{CO_2}$ sampling error, half of all monthly 1°x1° grid cells are found where the local range in daily mean $p\mathrm{CO_2}$ variability exceeds 25 μatm; for grid cells with a negative $p\mathrm{CO_2}$ sampling error, this only applies to one third of all grid cells (Fig. 9a, b).

The ratio of the absolute $p\mathrm{CO_2}$ sampling error to the range in daily mean $p\mathrm{CO_2}$ points to the dominant type of spatio-temporal variability for each monthly 1°x1° grid cell. While a ratio smaller than one indicates that the range in daily mean $p\mathrm{CO_2}$ dominates, a ratio larger than one means that sub-grid cell or diurnal variability dominate the $p\mathrm{CO_2}$ sampling error at that location. In E3SM, 82% of all monthly 1°x1° grid cells with a positive sampling error have a ratio smaller than one (Fig. 9d), and the important role of daily variability for these locations is in line with the spatial agreement between Fig. 8 and regions of high $p\mathrm{CO_2}$ variability in Figs. 6 & 7. For locations with a negative sampling error, only 49% of all monthly 1°x1° grid cells have a ratio smaller than one (Fig. 9c), illustrating the complex relationship between simulated spatio-temporal $p\mathrm{CO_2}$ variability and $p\mathrm{CO_2}$ sampling error in many parts of the Southern Ocean.

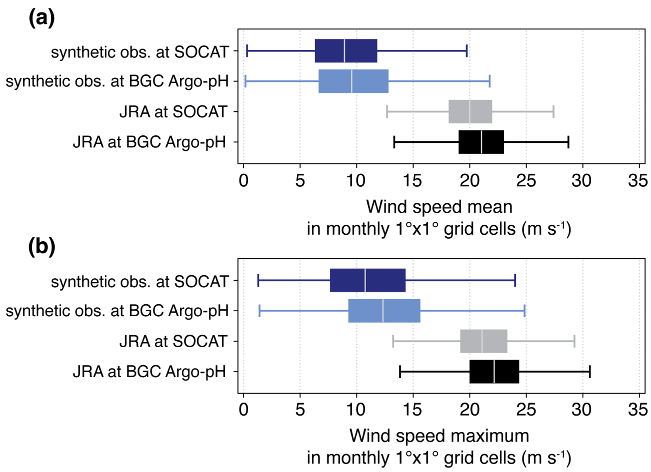

Figure 10. Box plot of the (a) wind speed mean (m s^{-1}) and (b) wind speed maximum (m s^{-1}) in all monthly 1°x1° grid cells between 2014 and 2023 with at least one observation (see Fig. 1) for synthetic observations at SOCAT sampling sites (dark blue), synthetic observations at BGC Argo-pH sampling sites (light blue), JRA at SOCAT sampling sites (grey) and JRA at BGC Argo-pH sampling sites (black). To obtain the distributions of synthetic observations at SOCAT and BGC Argo-pH sampling sites, we have used synthetic wind speed observations at historical sampling sites of $p\mathrm{CO}_2$ (see section 2.2). To obtain the JRA distributions, we have used the 3-hourly data of all JRA grid cells within each monthly 1°x1° grid cell. The comparison of the respective blue and grey bars thus highlights undersampling during high-wind events.

4 Discussion

Using an ocean model to quantify the Southern Ocean $p\mathrm{CO}_2$ sampling error, we find that reconstructed observations constrained by historical sampling coverage underestimate the true monthly mean $p\mathrm{CO}_2$ by, on average, 13–14 μatm, with biases in individual 1°x1° grid cells reaching values more than ten times larger. This average $p\mathrm{CO}_2$ sampling error is thus substantial, exceeding the accuracy required of ship-based $p\mathrm{CO}_2$ observations to be included in gridded SOCAT products (<5 μatm; Bakker et al., 2016) and the systematic error associated with float-derived $p\mathrm{CO}_2$ observations (∼3.5-11 μatm; Williams et al., 2017; Gray et al., 2018). The $p\mathrm{CO}_2$ sampling error is at least 33% of the seasonal $p\mathrm{CO}_2$ amplitude derived from monthly means of various $p\mathrm{CO}_2$ data products and ocean models in the seasonally ice-covered Southern Ocean (∼30-40 μatm), and is almost 100% of the $p\mathrm{CO}_2$ seasonal amplitude in the subpolar seasonally stratified regions (∼15 μatm) (Hauck et al., 2023a). Considering the large simulated sub-monthly and sub-grid cell $p\mathrm{CO}_2$ variability in E3SM, our findings underscore how incomplete observational coverage can skew our assessment of $p\mathrm{CO}_2$ seasonality (Monteiro et al., 2015). While the magnitude of the simulated sub-monthly $p\mathrm{CO}_2$ variability in E3SM is in line with existing observations (Sutton et al., 2014; OOI, 2015; Sutton et al., 2021; Robache and Schmitt, 2026), high-frequency observations remain sparse, especially for the regions with highest simulated variability in the high southern latitudes and off the Patagonian shelf. This lack of data currently prevents a more

https://doi.org/10.5194/egusphere-2026-4623
Preprint. Discussion started: 10 August 2026

comprehensive evaluation of high-frequency pCO_2 variability in E3SM and a more robust estimation of the pCO_2 sampling error.

In E3SM, both the average magnitude and the sign of the Southern Ocean pCO_2 sampling error remain largely unchanged when comparing an assessment only using ship-based observations (SOCAT) to one merging ship-based and float-based data (SOCAT + BGC Argo-pH). Ship-based observations are known to be biased to non-winter months and non-windy conditions (Fig. 2 and Bakker et al., 2016). Indeed, using our synthetic observations to compare mean and maximum wind speeds captured by historical SOCAT coverage to those in the Japanese atmospheric reanalysis (Tsujino et al., 2018) reveals that ship-based observations undersample when wind speeds are high (Fig. 10). Maybe surprisingly, the historical observational coverage of BGC Argo-pH is also biased towards low winds (Fig. 10). Since storms are pervasive in the Southern Ocean (Nissen et al., 2025) and can be associated with high-pCO_2 anomalies (Nicholson et al., 2022; Carranza et al., 2024; Christensen et al., 2026; Dombret et al., 2026), such skewed distributions towards low-pCO_2 values can, at least partly, explain the simulated negative sampling error in the synthetic observations.

Any Southern Ocean pCO_2 sampling error has potential implications for mapped pCO_2 data products (e.g., Landschützer et al., 2013; Gregor and Gruber, 2021; Gloege et al., 2022; Zeng et al., 2022) and ultimately assessments of the Southern Ocean and global ocean carbon sink (Hauck et al., 2023a; Friedlingstein et al., 2026). In E3SM, the overall lower pCO_2 values in the reconstructed synthetic observations compared to the model truth imply that oceanic CO_2 uptake is overestimated when derived from real-world observations. In other words, oceanic CO_2 uptake would be smaller if observational coverage was perfect in space and time. Recently, Dombret et al. (2026) showed that not adequately considering synoptic variability in winds and atmospheric pressure in air-sea CO_2 flux calculations leads to overestimates of oceanic CO_2 uptake mainly in the Southern Ocean, which is consistent with our findings. It remains unclear whether machine learning algorithms used to create gap-filled pCO_2 data products could, at least partly, compensate for the overall negative sampling error or what additional observational coverage would be necessary to achieve this. But since these routines are sensitive to the pCO_2 distributions used to train the machine learning algorithms (e.g., Hauck et al., 2023b; Fay et al., 2025), our results suggest that algorithms based on the raw pCO_2 (or fCO_2) observations, rather than on the monthly 1°x1° gridded SOCAT product, may have an advantage by preserving more of the underlying pCO_2 variability (e.g., Rödenbeck et al., 2022). Still, it is reasonable to assume that a negative sampling error would at least partially be sustained in mapped pCO_2 data products and propagate into derived CO_2 flux estimates.

5 Conclusions

Quantifying the uncertainty in surface ocean pCO_2 resulting from incomplete spatial or temporal coverage at the monthly 1°x1° scale, our findings highlight a previously unquantified source of uncertainty in the gridded pCO_2 data products underlying the vast majority of our estimates of the Southern Ocean carbon sink (Bakker et al., 2016; Hauck et al., 2023a; Friedlingstein et al., 2026). The pCO_2 sampling error quantified in this study is substantial, exceeding other sources of uncertainty relevant to constructing gridded pCO_2 data products, e.g., the sampling accuracy of ship-based or float-based pCO_2 observations (Bakker et al., 2016; Williams et al., 2017; Wanninkhof et al., 2019; Steinhoff et al., 2025). As long as complete spatial and temporal

https://doi.org/10.5194/egusphere-2026-4623
Preprint. Discussion started: 10 August 2026

coverage at the monthly 1°x1° scale remains limited by available resources, the pCO_2 sampling error is impossible to quantify with observations alone. Our study adds to the growing body of work that uses synthetic observations from global ocean models to quantify uncertainties in Southern Ocean pCO_2 distributions resulting from gaps in spatial or temporal coverage (e.g., Hauck et al., 2023b; Heimdal et al., 2024; Behncke et al., 2026). By more realistically extracting synthetic pCO_2 observations from a global ocean model with eddy-permitting resolution in the Southern Ocean, our synthetic datasets can better represent the snapshot nature of real-world observations and the incomplete historical observational coverage at the sub-monthly and sub-1°x1°-grid-cell scale. Our study thus highlights a critical shortcoming of studies using time-averaged output from models with comparatively coarser horizontal grid resolution.

Our findings underscore the need for several follow-up steps to deepen our understanding of how incomplete observational coverage biases estimates of the global ocean carbon sink. Applying machine learning algorithms, such as those currently used to construct pCO_2 data products for the Global Carbon Budget (Friedlingstein et al., 2026), to our improved synthetic pCO_2 datasets will allow us to quantify how sensitive mapped climatological and time-varying Southern Ocean pCO_2 fields are to incomplete observational coverage at the monthly 1°x1° scale. By considering other error sources, e.g., random or systematic errors of pCO_2 observations, such an exercise could also facilitate a comprehensive uncertainty assessment of pCO_2-derived air-sea CO_2 fluxes in a coherent model testbed. Repeating our analysis in different ocean models will give insights into which of our findings are specific to the Energy Exascale Earth System Model. Importantly, this would not require the full implementation of an observing system as done in Nissen et al. (2024). Providing any ocean model, but ideally those with at least eddy-permitting resolution, a list of locations and times of historical surface ocean pCO_2 measurements and extracting pCO_2 snapshots from the nearest model grid cell during the simulation would be sufficient. Besides facilitating a multi-model comparison and an assessment of how a more realistic extraction of synthetic observations affects the findings of previous studies (e.g., Hauck et al., 2023b; Heimdal et al., 2024; Behncke et al., 2026), these steps would also enable the quantification of the global pCO_2 sampling error. Until then, it remains unclear whether current sampling efforts in other regions, with either lower (e.g., subtropics) or comparable (e.g., North Atlantic) storm activity and associated wind variability, are sufficient to minimize the pCO_2 sampling error. Similarly, future work should also assess to what extent undersampling during high-wind events affects our ship-based or float-based understanding of other biogeochemical variables in the Southern Ocean and elsewhere (e.g., oxygen, nitrous oxide, or chlorophyll; Sharp et al., 2023; Nissen et al., 2025; Kelly et al., 2026). Lastly, additional high-frequency observations would allow for a more detailed evaluation of simulated temporal pCO_2 variability in ocean models and a more robust quantification of the pCO_2 sampling error. Ultimately, model testbeds are indispensable for observing system design, provided they capture all relevant scales of variability and generate synthetic observations in a realistic manner.

Code and data availability. The model source code of E3SMv2 including synthetic biogeochemical float capabilities is available on Zenodo: https://doi.org/10.5281/zenodo.10094349 (Energy Exascale Earth System Model Program, 2023). The data underlying the findings of this paper are available on Zenodo: https://doi.org/10.5281/zenodo.21289725 (Nissen, 2026b). The analysis scripts used to post-process E3SM model output and produce the figures in this paper are available on GitHub (Nissen, 2026a). A final version of these scripts will be archived on Zenodo upon acceptance of this paper.

Author contributions. CN conceived the study, performed the analysis, and wrote the first version of the paper. CN, NSL and MM acquired the funding. MM ran the underlying E3SM simulation. All authors contributed to the interpretation of the findings and to the writing of the paper.

Competing interests. The authors declare there are no conflicts of interest for this manuscript.

Acknowledgements. CN, NSL, and MM are grateful for support by the US Department of Energy (Grant DE-SC0025505). ARG acknowledges support from NSF through Awards 2332379, 1946578, and 2110258 and from NOAA through Award NA24OARX431C0057. This publication is partially funded by the Cooperative Institute for Climate, Ocean, & Ecosystem Studies (CICOES) under NOAA Cooperative Agreements NA20OAR4320271 and NA25OARX432C0012, Contribution No. 2026-1571. This research used resources of the National Energy Research Scientific Computing Center (NERSC), a US Department of Energy Office of Science User Facility located at Lawrence Berkeley National Laboratory and high-performance computing clusters provided by the BER Earth System Modeling program and operated by Pacific Northwest National Laboratory and the Laboratory Computing Resource Center at Argonne National Laboratory. The Surface Ocean CO_2 Atlas (SOCAT) is an international effort, endorsed by the SCOR Infrastructural Project International Ocean Carbon Coordination Project (IOCCP) and the Surface Ocean Lower-Atmosphere Study (SOLAS), to deliver a uniform, quality-controlled surface ocean CO_2 database. The many researchers and funding agencies responsible for the collection of data and quality control are thanked for their contributions to SOCAT. Argo data were collected and made freely available by the international Argo project and the national programs that contribute to it. The mooring data from the Argentine basin is based upon work supported by the Ocean Observatories Initiative (OOI), a major facility fully funded by the US National Science Foundation under Cooperative Agreement No. 2244833, and the Woods Hole Oceanographic Institution OOI Program Office.

References

Argo: Argo float data and metadata from Global Data Assembly Centre (Argo GDAC) - Snapshot of BGC Sprof data files of January 9, 2024, SEANOE, https://doi.org/10.17882/42182#107469, 2024.

Bakker, D. C. E., Pfeil, B., Landa, C. S., Metzl, N., O'Brien, K. M., Olsen, A., Smith, K., Cosca, C., Harasawa, S., Jones, S. D., Nakaoka, S.-i., Nojiri, Y., Schuster, U., Steinhoff, T., Sweeney, C., Takahashi, T., Tilbrook, B., Wada, C., Wanninkhof, R., Alin, S. R., Balestrini, C. F., Barbero, L., Bates, N. R., Bianchi, A. A., Bonou, F., Boutin, J., Bozec, Y., Burger, E. F., Cai, W.-J., Castle, R. D., Chen, L., Chierici, M., Currie, K., Evans, W., Featherstone, C., Feely, R. A., Fransson, A., Goyet, C., Greenwood, N., Gregor, L., Hankin, S., Hardman-Mountford, N. J., Harlay, J., Hauck, J., Hoppema, M., Humphreys, M. P., Hunt, C. W., Huss, B., Ibánhez, J. S. P., Johannessen, T., Keeling, R., Kitidis, V., Körtzinger, A., Kozyr, A., Krasakopoulou, E., Kuwata, A., Landschützer, P., Lauvset, S. K., Lefèvre, N., Lo Monaco, C., Manke, A., Mathis, J. T., Merlivat, L., Millero, F. J., Monteiro, P. M. S., Munro, D. R., Murata, A., Newberger, T., Omar, A. M., Ono, T., Paterson, K., Pearce, D., Pierrot, D., Robbins, L. L., Saito, S., Salisbury, J., Schlitzer, R., Schneider, B., Schweitzer, R., Sieger, R., Skjelvan, I., Sullivan, K. F., Sutherland, S. C., Sutton, A. J., Tadokoro, K., Telszewski, M., Tuma, M., van Heuven, S. M. A. C., Vandemark, D., Ward, B., Watson, A. J., and Xu, S.: A multi-decade record of high-quality fCO_2 data in version 3 of the Surface Ocean CO_2 Atlas (SOCAT), Earth System Science Data, 8, 383–413, https://doi.org/10.5194/essd-8-383-2016, 2016.

Bakker, D. C. E., Alin, S. R., Bates, N., Becker, M., Gkritzalis, T., Jones, S. D., Kozyr, A., Lauvset, S. K., Metzl, N., Nakaoka, S.-i., O'Brien, K. M., Olsen, A., Pierrot, D., Steinhoff, T., Sutton, A. J., Takao, S., Tilbrook, B., Wada, C., Wanninkhof, R., Akl, J., Arbilla, L. A., Arruda, R., Azetsu-Scott, K., Barbero, L., Beatty, C. M., Berghoff, C. F., Bittig, H. C., Burger, E. F., Campbell, K., Cardin, V., Collins, A., Coppola, L., Cronin, M., Cross, J. N., Currie, K. I., Emerson, S. R., Enright, M. P., Enyo, K., Evans, W., Feely, R. A., Flohr, A., Gehrung, M., Glockzin, M., González-Dávila, M., Hamnca, S., Hartman, S. E., Howden, S. D., Kam, K., Kamb, L., Körtzinger, A., Kosugi, N., Lefèvre, N., Lo Monaco, C., Macovei, V. A., Maenner Jones, S., Manalang, D., Martz, T. R., Mdokwana, B., Monacci, N. M., Monteiro, P. M. S., Mordy, C., Morell, J. M., Murata, A., Neill, C., Noh, J.-H., Nojiri, Y., Ohman, M. D., Olivier, L., Ono, T., Petersen, W., Plueddemann, A. J., Prytherch, J., Rehder, G., Rutgersson, A., Santana-Casiano, J. M., Schlitzer, R., Send, U., Skjelvan, I., Sullivan, K. F., T'Jampens, M., Tadokoro, K., Telszewski, M., Theetaert, H., Tsanwani, M., Vandemark, D., van Ooijen, E., Veccia, M. H., Voynova, Y. G., Wang, H., Weller, R. A., and Woosley, R. J.: Surface Ocean CO_2 Atlas Database Version 2024 (SOCATv2024) (NCEI Accession 0293257), NOAA National Centers for Environmental Information, accessed on April 7, 2025, https://doi.org/10.25921/9wpn-th28, 2024.

Behncke, J., Landschützer, P., and Tanhua, T.: A detectable change in the air-sea CO_2 flux estimate from sailboat measurements, Scientific Reports, 14, 3345, https://doi.org/10.1038/s41598-024-53159-0, 2024.

Behncke, J., Ilyina, T., Chegini, F., and Landschützer, P.: Improved air-sea CO_2 flux estimates from sailboat measurements, Science advances, 12, eadz1502, https://doi.org/10.1126/sciadv.adz1502, 2026.

Bellenger, H., Bopp, L., Ethé, C., Ho, D., Duvel, J. P., Flavoni, S., Guez, L., Kataoka, T., Perrot, X., Parc, L., and Watanabe, M.: Sensitivity of the Global Ocean Carbon Sink to the Ocean Skin in a Climate Model, Journal of Geophysical Research: Oceans, 128, 1–22, https://doi.org/10.1029/2022JC019479, 2023.

Bushinsky, S. M., Landschützer, P., Rödenbeck, C., Gray, A. R., Baker, D., Mazloff, M. R., Resplandy, L., Johnson, K. S., and Sarmiento, J. L.: Reassessing Southern Ocean Air-Sea CO_2 Flux Estimates With the Addition of Biogeochemical Float Observations, Global Biogeochemical Cycles, 33, 1370–1388, https://doi.org/10.1029/2019GB006176, 2019.

Carranza, M. M., Long, M. C., Di Luca, A., Fassbender, A. J., Johnson, K. S., Takeshita, Y., Mongwe, P., and Turner, K. E.: Extratropical storms induce carbon outgassing over the Southern Ocean, npj Climate and Atmospheric Science, 7, 106, https://doi.org/10.1038/s41612-024-00657-7, 2024.

Christensen, K., Lovenduski, N. S., Conlon, L., Maltrud, M., and Nissen, C.: Diagnosing the influence of Southern Ocean storms on air-sea carbon dioxide flux from synthetic floats: A modeling study, ESS Open Archive, https://doi.org/10.22541/essoar.15006783/v1, 2026.

DeVries, T., Yamamoto, K., Wanninkhof, R., Gruber, N., Hauck, J., Müller, J. D., Bopp, L., Carroll, D., Carter, B., Chau, T., Doney, S. C., Gehlen, M., Gloege, L., Gregor, L., Henson, S., Kim, J. H., Iida, Y., Ilyina, T., Landschützer, P., Le Quéré, C., Munro, D., Nissen, C., Patara, L., Pérez, F. F., Resplandy, L., Rodgers, K. B., Schwinger, J., Séférian, R., Sicardi, V., Terhaar, J., Triñanes, J., Tsujino, H., Watson, A., Yasunaka, S., and Zeng, J.: Magnitude, Trends, and Variability of the Global Ocean Carbon Sink From 1985 to 2018, Global Biogeochemical Cycles, 37, https://doi.org/10.1029/2023GB007780, 2023.

Djeutchouang, L. M., Chang, N., Gregor, L., Vichi, M., and Monteiro, P. M. S.: The sensitivity of $p\mathrm{CO_2}$ reconstructions to sampling scales across a Southern Ocean sub-domain: a semi-idealized ocean sampling simulation approach, Biogeosciences, 19, 4171–4195, https://doi.org/10.5194/bg-19-4171-2022, 2022.

Dombret, J., Bellenger, H., Perrot, X., Parc, L., Kwiatkowski, L., Chevallier, F., Bopp, L., Gehlen, M., Séférian, R., Berthet, S., and Orr, J. C.: Data-based estimates of ocean carbon uptake biased high from neglect of submonthly atmospheric pressure variability, Biogeosciences, 23, 4133–4143, https://doi.org/10.5194/bg-23-4133-2026, 2026.

Dong, Y., Bakker, D. C. E., and Landschützer, P.: Accuracy of Ocean CO_2 Uptake Estimates at a Risk by a Reduction in the Data Collection, Geophysical Research Letters, 51, https://doi.org/10.1029/2024GL108502, 2024.

Energy Exascale Earth System Model Program: Energy Exascale Earth System Model (E3SMv2) code with Argo float simulator, https://doi.org/10.5281/zenodo.10094349, Zenodo, 2023.

Eveleth, R., Cassar, N., Doney, S., Munro, D., and Sweeney, C.: Biological and physical controls on O_2/Ar, Ar and pCO_2 variability at the Western Antarctic Peninsula and in the Drake Passage, Deep Sea Research Part II: Topical Studies in Oceanography, 139, 77–88, https://doi.org/10.1016/j.dsr2.2016.05.002, 2017.

Fay, A. R., Heimdal, T. H., Acquaviva, V., Shaum, A. P., and McKinley, G. A.: Sensitivity of Ocean Carbon Sink Estimates to Rare Observations, Geophysical Research Letters, 52, https://doi.org/10.1029/2025GL117961, 2025.

Friedlingstein, P., O'Sullivan, M., Jones, M. W., Andrew, R. M., Bakker, D. C. E., Hauck, J., Landschützer, P., Le Quéré, C., Li, H., Luijkx, I. T., Peters, G. P., Peters, W., Pongratz, J., Schwingshackl, C., Sitch, S., Canadell, J. G., Ciais, P., Aas, K., Alin, S. R., Anthoni, P., Barbero, L., Bates, N. R., Bellouin, N., Benoit-Cattin, A., Berghoff, C. F., Bernardello, R., Bopp, L., Brasika, I. B. M., Chamberlain, M. A., Chandra, N., Chevallier, F., Chini, L. P., Collier, N. O., Colligan, T. H., Cronin, M., Djeutchouang, L. M., Dou, X., Enright, M. P., Enyo, K., Erb, M., Evans, W., Feely, R. A., Feng, L., Ford, D. J., Foster, A., Fransner, F., Gasser, T., Gehlen, M., Gkritzalis, T., Goncalves De Souza, J., Grassi, G., Gregor, L., Gruber, N., Guenet, B., Gürses, Ö., Harrington, K., Harris, I., Heinke, J., Hurtt, G. C., Iida, Y., Ilyina, T., Ito, A., Jacobson, A. R., Jain, A. K., Jarníková, T., Jersild, A., Jiang, F., Jones, S. D., Kato, E., Keeling, R. F., Klein Goldewijk, K., Knauer, J., Kong, Y., Korsbakken, J. I., Koven, C., Kunimitsu, T., Lan, X., Liu, J., Liu, Z., Liu, Z., Lo Monaco, C., Ma, L., Marland, G., McGuire, P. C., McKinley, G. A., Melton, J. R., Monacci, N., Monier, E., Morgan, E. J., Munro, D. R., Müller, J. D., Nakaoka, S.-I., Nayagam, L. R., Niwa, Y., Nutzel, T., Olsen, A., Omar, A. M., Pan, N., Pandey, S., Pierrot, D., Qin, Z., Regnier, P., Rehder, G., Resplandy, L., Roobaert, A., Rosan, T. M., Rödenbeck, C., Schwinger, J., Skjelvan, I., Smallman, T. L., Spada, V., Sreeush, M. G., Sun, Q., Sutton, A. J., Sweeney, C., Swingedouw, D., Séférian, R., Takao, S., Tatebe, H., Tian, H., Tian, X., Tilbrook, B., Tsujino, H., Tubiello, F., van

Ooijen, E., van der Werf, G. R., van de Velde, S. J., Walker, A. P., Wanninkhof, R., Yang, X., Yuan, W., Yue, X., and Zeng, J.: Global Carbon Budget 2025, Earth System Science Data, 18, 3211–3288, https://doi.org/10.5194/essd-18-3211-2026, 2026.

Gloege, L., Yan, M., Zheng, T., and McKinley, G. A.: Improved Quantification of Ocean Carbon Uptake by Using Machine Learning to Merge Global Models and $p\mathrm{CO_2}$ Data, Journal of Advances in Modeling Earth Systems, 14, 1–19, https://doi.org/10.1029/2021MS002620, 2022.

Golaz, J. C., Van Roekel, L. P., Zheng, X., Roberts, A. F., Wolfe, J. D., Lin, W., Bradley, A. M., Tang, Q., Maltrud, M. E., Forsyth, R. M., Zhang, C., Zhou, T., Zhang, K., Zender, C. S., Wu, M., Wang, H., Turner, A. K., Singh, B., Richter, J. H., Qin, Y., Petersen, M. R., Mametjanov, A., Ma, P. L., Larson, V. E., Krishna, J., Keen, N. D., Jeffery, N., Hunke, E. C., Hannah, W. M., Guba, O., Griffin, B. M., Feng, Y., Engwirda, D., Di Vittorio, A. V., Dang, C., Conlon, L. A. M., Chen, C. C. J., Brunke, M. A., Bisht, G., Benedict, J. J., Asay-Davis, X. S., Zhang, Y., Zhang, M., Zeng, X., Xie, S., Wolfram, P. J., Vo, T., Veneziani, M., Tesfa, T. K., Sreepathi, S., Salinger, A. G., Reeves Eyre, J. E., Prather, M. J., Mahajan, S., Li, Q., Jones, P. W., Jacob, R. L., Huebler, G. W., Huang, X., Hillman, B. R., Harrop, B. E., Foucar, J. G., Fang, Y., Comeau, D. S., Caldwell, P. M., Bartoletti, T., Balaguru, K., Taylor, M. A., McCoy, R. B., Leung, L. R., and Bader, D. C.: The DOE E3SM Model Version 2: Overview of the Physical Model and Initial Model Evaluation, Journal of Advances in Modeling Earth Systems, 14, 1–51, https://doi.org/10.1029/2022MS003156, 2022.

Gray, A. R., Johnson, K. S., Bushinsky, S. M., Riser, S. C., Russell, J. L., Talley, L. D., Wanninkhof, R., Williams, N. L., and Sarmiento, J. L.: Autonomous Biogeochemical Floats Detect Significant Carbon Dioxide Outgassing in the High-Latitude Southern Ocean, Geophysical Research Letters, 45, 9049–9057, https://doi.org/10.1029/2018GL078013, 2018.

Gregor, L. and Gruber, N.: OceanSODA-ETHZ: a global gridded data set of the surface ocean carbonate system for seasonal to decadal studies of ocean acidification, Earth System Science Data, 13, 777–808, https://doi.org/10.5194/essd-13-777-2021, 2021.

Gregor, L., Shutler, J., and Gruber, N.: High-Resolution Variability of the Ocean Carbon Sink, Global Biogeochemical Cycles, 38, 1–27, https://doi.org/10.1029/2024GB008127, 2024.

Hauck, J., Gregor, L., Nissen, C., Patara, L., Hague, M., Mongwe, P., Bushinsky, S., Doney, S. C., Gruber, N., Le Quéré, C., Manizza, M., Mazloff, M., Monteiro, P. M. S., and Terhaar, J.: The Southern Ocean Carbon Cycle 1985–2018: Mean, Seasonal Cycle, Trends, and Storage, Global Biogeochemical Cycles, 37, 1–55, https://doi.org/10.1029/2023GB007848, 2023a.

Hauck, J., Nissen, C., Landschützer, P., Rödenbeck, C., Bushinsky, S., and Olsen, A.: Sparse observations induce large biases in estimates of the global ocean $\mathrm{CO_2}$ sink: an ocean model subsampling experiment, Philosophical Transactions of the Royal Society A: Mathematical, Physical and Engineering Sciences, 381, https://doi.org/10.1098/rsta.2022.0063, 2023b.

Heimdal, T. H. and McKinley, G. A.: The importance of adding unbiased Argo observations to the ocean carbon observing system, Scientific Reports, 14, 19 763, https://doi.org/10.1038/s41598-024-70617-x, 2024.

Heimdal, T. H., McKinley, G. A., Sutton, A. J., Fay, A. R., and Gloege, L.: Assessing improvements in global ocean $p\mathrm{CO_2}$ machine learning reconstructions with Southern Ocean autonomous sampling, Biogeosciences, 21, 2159–2176, https://doi.org/10.5194/bg-21-2159-2024, 2024.

Kelly, C. L., Chang, B. X., Emmanuelli, A. F., Park, E. R., Macdonald, A. M., and Nicholson, D. P.: Low-pressure storms drive nitrous oxide emissions in the Southern Ocean, Nature Communications, 17, 2037, https://doi.org/10.1038/s41467-026-68744-2, 2026.

Landschützer, P., Gruber, N., Bakker, D. C. E., Schuster, U., Nakaoka, S., Payne, M. R., Sasse, T. P., and Zeng, J.: A neural network-based estimate of the seasonal to inter-annual variability of the Atlantic Ocean carbon sink, Biogeosciences, 10, 7793–7815, https://doi.org/10.5194/bg-10-7793-2013, 2013.

https://doi.org/10.5194/egusphere-2026-4623
Preprint. Discussion started: 10 August 2026

Long, M. C., Moore, J. K., Lindsay, K., Levy, M., Doney, S. C., Luo, J. Y., Krumhardt, K. M., Letscher, R. T., Grover, M., and Sylvester, Z. T.: Simulations With the Marine Biogeochemistry Library (MARBL), Journal of Advances in Modeling Earth Systems, 13, https://doi.org/10.1029/2021MS002647, 2021.

Monteiro, P. M. S., Gregor, L., Lévy, M., Maenner, S., Sabine, C. L., and Swart, S.: Intraseasonal variability linked to sampling alias in air-sea CO_2 fluxes in the Southern Ocean, Geophysical Research Letters, 42, 8507–8514, https://doi.org/10.1002/2015GL066009, 2015.

Nicholson, S.-A., Whitt, D. B., Fer, I., du Plessis, M. D., Lebéhot, A. D., Swart, S., Sutton, A. J., and Monteiro, P. M. S.: Storms drive outgassing of CO_2 in the subpolar Southern Ocean, Nature Communications, 13, 158, https://doi.org/10.1038/s41467-021-27780-w, 2022.

Nissen, C.: Analysis scripts for "Quantifying the Southern Ocean pCO_2 sampling error with synthetic observations from an ocean model" [Data set], GitHub, https://github.com/cara-nissen/E3SM_pCO2_sampling_error, 2026a.

Nissen, C.: E3SM model data: Quantifying the Southern Ocean pCO_2 sampling error with synthetic observations from an ocean model [Dataset], https://doi.org/10.5281/zenodo.21289725, Zenodo, 2026b.

Nissen, C., Lovenduski, N. S., Maltrud, M., Gray, A. R., Takano, Y., Falcinelli, K., Sauvé, J., and Smith, K.: LIGHT-bgcArgo-1.0: using synthetic float capabilities in E3SMv2 to assess spatiotemporal variability in ocean physics and biogeochemistry, Geoscientific Model Development, 17, 6415–6435, https://doi.org/10.5194/gmd-17-6415-2024, 2024.

Nissen, C., Clow, G. L., Lovenduski, N. S., Turner, K. E., Carranza, M. M., and Krumhardt, K. M.: The Imprint of Southern Ocean Storms on Modeled Surface Chlorophyll, Their Drivers and Satellite Biases, Global Biogeochemical Cycles, 39, https://doi.org/10.1029/2025GB008550, 2025.

OOI: NSF Ocean Observatories Initiative, ERDDAP, https://doi.org/10.58046/OOI-GA01SUMO. Accessed on June 10, 2026, 2015.

Patara, L., Rieck, J. K., Hauck, J., Ödalen, M., Oschlies, A., and Özgür Gürses: Stronger Southern Ocean Anthropogenic Carbon Uptake in Eddying Ocean Simulations, Journal of Climate, 39, 2017 – 2037, https://doi.org/10.1175/JCLI-D-25-0198.1, 2026.

Petersen, M. R., Asay-Davis, X. S., Berres, A. S., Chen, Q., Feige, N., Hoffman, M. J., Jacobsen, D. W., Jones, P. W., Maltrud, M. E., Price, S. F., Ringler, T. D., Streletz, G. J., Turner, A. K., Van Roekel, L. P., Veneziani, M., Wolfe, J. D., Wolfram, P. J., and Woodring, J. L.: An Evaluation of the Ocean and Sea Ice Climate of E3SM Using MPAS and Interannual CORE-II Forcing, Journal of Advances in Modeling Earth Systems, p. 2018MS001373, https://doi.org/10.1029/2018MS001373, 2019.

Ringler, T., Petersen, M., Higdon, R. L., Jacobsen, D., Jones, P. W., and Maltrud, M.: A multi-resolution approach to global ocean modeling, Ocean Modelling, 69, 211–232, https://doi.org/10.1016/j.ocemod.2013.04.010, 2013.

Robache, K. and Schmitt, F. G.: Lagrangian Scaling and Intermittency of Turbulent CARbon Interface OCean Atmosphere (CARIOCA) Time Series in the Southern Ocean, Journal of Geophysical Research: Oceans, 131, https://doi.org/10.1029/2025JC023080, 2026.

Rödenbeck, C., DeVries, T., Hauck, J., Le Quéré, C., and Keeling, R. F.: Data-based estimates of interannual sea–air CO_2 flux variations 1957–2020 and their relation to environmental drivers, Biogeosciences, 19, 2627–2652, https://doi.org/10.5194/bg-19-2627-2022, 2022.

Roobaert, A., Ford, D. J., Sreeush, M. G., Mckinley, G. A., Hauck, J., and Fay, A. R.: Reconciling ocean carbon uptake estimates : a multi-model assessment of surface ocean CO_2 reconstruction skill within the SOCOMv2 initiative, ESS Open Archive, https://doi.org/10.22541/essoar.15003624/v1, 2026.

Sabine, C. L., Hankin, S., Koyuk, H., Bakker, D. C. E., Pfeil, B., Olsen, A., Metzl, N., Kozyr, A., Fassbender, A., Manke, A., Malczyk, J., Akl, J., Alin, S. R., Bellerby, R. G. J., Borges, A., Boutin, J., Brown, P. J., Cai, W.-J., Chavez, F. P., Chen, A., Cosca, C., Feely, R. A., González-Dávila, M., Goyet, C., Hardman-Mountford, N., Heinze, C., Hoppema, M., Hunt, C. W., Hydes, D., Ishii, M., Johannessen, T., Key, R. M., Körtzinger, A., Landschützer, P., Lauvset, S. K., Lefèvre, N., Lenton, A., Lourantou, A., Merlivat, L., Midorikawa, T., Mintrop, L., Miyazaki, C., Murata, A., Nakadate, A., Nakano, Y., Nakaoka, S., Nojiri, Y., Omar, A. M., Padin, X. A., Park, G.-H., Paterson, K.,

https://doi.org/10.5194/egusphere-2026-4623
Preprint. Discussion started: 10 August 2026

Perez, F. F., Pierrot, D., Poisson, A., Ríos, A. F., Salisbury, J., Santana-Casiano, J. M., Sarma, V. V. S. S., Schlitzer, R., Schneider, B., Schuster, U., Sieger, R., Skjelvan, I., Steinhoff, T., Suzuki, T., Takahashi, T., Tedesco, K., Telszewski, M., Thomas, H., Tilbrook, B., Vandemark, D., Veness, T., Watson, A. J., Weiss, R., Wong, C. S., and Yoshikawa-Inoue, H.: Surface Ocean CO_2 Atlas (SOCAT) gridded data products, Earth System Science Data, 5, 145–153, https://doi.org/10.5194/essd-5-145-2013, 2013.

Sarmiento, J. L., Johnson, K. S., Arteaga, L. A., Bushinsky, S. M., Cullen, H. M., Gray, A. R., Hotinski, R. M., Maurer, T. L., Mazloff, M. R., Riser, S. C., Russell, J. L., Schofield, O. M., and Talley, L. D.: The Southern Ocean carbon and climate observations and modeling (SOCCOM) project: A review, Progress in Oceanography, 219, 103 130, https://doi.org/10.1016/j.pocean.2023.103130, 2023.

Shadwick, E. H., Wynn-Edwards, C. A., Matear, R. J., Jansen, P., Schulz, E., and Sutton, A. J.: Observed amplification of the seasonal CO_2 cycle at the Southern Ocean Time Series, Frontiers in Marine Science, 10, 1–11, https://doi.org/10.3389/fmars.2023.1281854, 2023.

Sharp, J. D., Fassbender, A. J., Carter, B. R., Johnson, G. C., Schultz, C., and Dunne, J. P.: GOBAI-O_2 : temporally and spatially resolved fields of ocean interior dissolved oxygen over nearly 2 decades, Earth System Science Data, 15, 4481–4518, https://doi.org/10.5194/essd-15-4481-2023, 2023.

Steinhoff, T., Gkritzalis, T., Jones, S., Macovei, V. A., Neill, C., Schuster, U., Akl, J., Arruda, R., Atamanchuk, D., Barry, M., Beaumont, L., Cantoni, C., Dickson, A., Fahning, J., Fought, J., Frangoulis, C., Gutiérrez-Loza, L., Hagan, C., Honkanen, M., Kielosto, S., Kinski, N., Körtzinger, A., Landschützer, P., Lauvset, S. K., Lawrence-Slavas, N., Li, Q., Luchetta, A., Malarde, D., Paulsen, M., Ritschel, M., Rutgersson, A., Sanders, R., Shitashima, K., Spaulding, R., Stamataki, N., Stenbäck, K., Sutton, A., Tatkiewicz, W., Telszewski, M., Theetaert, H., Tilbrook, B., and Wanninkhof, R.: The ICOS OTC pCO_2 instrument intercomparison, Limnology and Oceanography: Methods, 23, 924–948, https://doi.org/10.1002/lom3.10727, 2025.

Sutton, A. J., Sabine, C. L., Trull, T., Dietrich, C., Maenner Jones, S., Musielewicz, S., Bott, R., and Osborne, J.: High-resolution ocean and atmosphere pCO_2 time-series measurements from mooring SOFS_142E_46S in the Indian Ocean, NCEI Accession 0118546, https://doi.org/10.3334/cdiac/otg.tsm_sofs_142w_46s. Accessed on June 10, 2026, 2014.

Sutton, A. J., Williams, N. L., and Tilbrook, B.: Constraining Southern Ocean CO_2 Flux Uncertainty Using Uncrewed Surface Vehicle Observations, Geophysical Research Letters, 48, 1–9, https://doi.org/10.1029/2020GL091748, 2021.

Tsujino, H., Urakawa, S., Nakano, H., Small, R. J., Kim, W. M., Yeager, S. G., Danabasoglu, G., Suzuki, T., Bamber, J. L., Bentsen, M., Böning, C. W., Bozec, A., Chassignet, E. P., Curchitser, E., Boeira Dias, F., Durack, P. J., Griffies, S. M., Harada, Y., Ilicak, M., Josey, S. A., Kobayashi, C., Kobayashi, S., Komuro, Y., Large, W. G., Le Sommer, J., Marsland, S. J., Masina, S., Scheinert, M., Tomita, H., Valdivieso, M., and Yamazaki, D.: JRA-55 based surface dataset for driving ocean–sea-ice models (JRA55-do), Ocean Modelling, 130, 79–139, https://doi.org/10.1016/j.ocemod.2018.07.002, 2018.

Turner, A. K., Lipscomb, W. H., Hunke, E. C., Jacobsen, D. W., Jeffery, N., Engwirda, D., Ringler, T. D., and Wolfe, J. D.: MPAS-Seaice (v1.0.0): sea-ice dynamics on unstructured Voronoi meshes, Geoscientific Model Development, 15, 3721–3751, https://doi.org/10.5194/gmd-15-3721-2022, 2022.

Wanninkhof, R., Pickers, P. A., Omar, A. M., Sutton, A., Murata, A., Olsen, A., Stephens, B. B., Tilbrook, B., Munro, D., Pierrot, D., Rehder, G., Santana-Casiano, J. M., Müller, J. D., Trinanes, J., Tedesco, K., O'Brien, K., Currie, K., Barbero, L., Telszewski, M., Hoppema, M., Ishii, M., González-Dávila, M., Bates, N. R., Metzl, N., Suntharalingam, P., Feely, R. A., ichiro Nakaoka, S., Lauvset, S. K., Takahashi, T., Steinhoff, T., and Schuster, U.: A surface ocean CO_2 reference network, SOCONET and associated marine boundary layer CO2 measurements, Frontiers in Marine Science, 6, https://doi.org/10.3389/fmars.2019.00400, 2019.

https://doi.org/10.5194/egusphere-2026-4623
Preprint. Discussion started: 10 August 2026

Williams, N. L., Juranek, L. W., Feely, R. A., Johnson, K. S., Sarmiento, J. L., Talley, L. D., Dickson, A. G., Gray, A. R., Wanninkhof, R., Russell, J. L., Riser, S. C., and Takeshita, Y.: Calculating surface ocean $p\mathrm{CO_2}$ from biogeochemical Argo floats equipped with pH: An uncertainty analysis, Global Biogeochemical Cycles, 31, 591–604, https://doi.org/10.1002/2016GB005541, 2017.

Wolfram, P. J., Ringler, T. D., Maltrud, M. E., Jacobsen, D. W., and Petersen, M. R.: Diagnosing Isopycnal Diffusivity in an Eddying, Idealized Midlatitude Ocean Basin via Lagrangian, in Situ, Global, High-Performance Particle Tracking (LIGHT), Journal of Physical Oceanography, 45, 2114–2133, https://doi.org/10.1175/JPO-D-14-0260.1, 2015.

Zeng, J., Iida, Y., Matsunaga, T., and Shirai, T.: Surface ocean $\mathrm{CO_2}$ concentration and air-sea flux estimate by machine learning with modelled variable trends, Frontiers in Marine Science, 9, 1–14, https://doi.org/10.3389/fmars.2022.989233, 2022.

Zhang, C., Wu, Y., Brown, P. J., Stappard, D., Silva, A. N., and Tyrrell, T.: A systematic bias in float pH leads to overestimation of derived $p\mathrm{CO_2}$ and underestimation of carbon uptake by the Southern Ocean, Scientific reports, 16, 1–15, https://doi.org/10.1038/s41598-026-43863-4, 2026.